ACES Asian Chemical Editorial Society

DOI: 10.1002/cnma.201800052

CHEMNANOMAT
Full Paper

SPECIAL ISSUE

Supported Metal Nanoparticles

Theoretical Investigation of Metal-Support Interactions on Ripening Kinetics of Supported Particles

Sulei Hu (胡素磊)[a, d] and Wei-Xue Li (李微雪)*[a, b, c]

Abstract: The stability of supported metal particles is one of the key issues for successful industrialization of catalysts. A theoretical study of Ostwald ripening of supported particles and its dependence on metal-support interactions, sublimation energy, and surface energy is reported. Two distinct metal-support interactions are differentiated: metal particle-support and metal atom-support. Although strong metal particle-support interaction (small contact angle) stabilizes the supported particles and improve the ripening resistance, strong metal atom-support interactions decrease the total activation energy and dramatically lower the onset temperature and half-life time of ripening, a fact that should be prevented. Moreover, supported particles with low surface energy and/or high sublimation energy of supported particles would have a high onset temperature and a long half-life time. Compared to the metal particle-support interaction and surface energy, the metal atom-support interaction and sublimation energy are most influential to the overall ripening resistance. The present work highlights the importance of interplay between two types of metal-support interactions on the overall stability of supported particles.

Introduction

Transition metal particles on supports are widely used to catalyse chemical reactions in heterogeneous catalysis.[1] It is often prepared at small size for higher surface area, which is particularly important for precious platinum group metals.[2] Exposed numerous low coordination sites and accompanied quantum size effect make the catalysts intrinsically more active and selective.[3] However, the cost is rapid increase of the specific surface energy destabilizing significantly the corresponding particles. To minimize the specific surface energy, small particles tend to sinter to the larger ones via particle migration and coalescence[4] and/or Ostwald ripening.[5] Slowing down the sintering rate and prolonging the life time of supported particles under reaction conditions are vital for industrialization of laboratory catalysts.

Sintering and stability of supported particles have been studied extensively in past. It was found that among others, varying surface structure and composition of supports can effectively improve the sintering resistance.[6] Taking Pt particles as example, the sintering occurred easily on inert alumina support,[7] but was inhibited in a large extent on more active ceria support.[8] Strong metal-support interaction (MSI) was essential here to stabilize the supported particles by forming strong Pt–O–Ce bond at the interface.[9] Recent studies indicate that strong MSI can also promote catalytic activity through so-called interface-confined effect[10] or electrical interaction.[11] On the other hand, MSI could not be too strong, since it might result in the formation of the metal-support solution, which deactivates the catalysts otherwise.[12] For particles in confined space, though particle migration and coalescence is prevented, growth of the particles still happened via Ostwald ripening through gas phase,[5,13] where corresponding sublimation energies matter. It was also reported that morphology[14] of supported particles affects the sintering process, due to the change of surface energy by adsorption of reactants.[15] Nevertheless, theoretical investigation of the metal-support interaction, sublimation energy and surface energy on Ostwald ripening are valuable, and quantitative study of their influence on ripening kinetics is not reported yet.

Ostwald ripening of supported metal particles describes the growth of the large particles with expense of the smaller ones, which has been extensively studied. In this process, the metal atoms detach from the smaller particles with higher chemical

[a] S. Hu (胡素磊), Prof. W.-X. Li (李微雪)
State Key Laboratory of Catalysis, Dalian Institute of Chemical Physics.
Chinese Academy of Sciences.
Dalian 116023, China
E-mail: wxli70@ustc.edu.cn
[b] Prof. W.-X. Li (李微雪)
Department of Chemical Physics, School of Chemistry and Materials Science,
iCHeM, CAS Excellence Center for Nanoscience
University of Science and Technology of China
Hefei 230026, China
[c] Prof. W.-X. Li (李微雪)
Hefei National Laboratory for Physical Sciences at the Microscale
University of Science and Technology of China
Hefei 230026, China
[d] S. Hu (胡素磊)
University of Chinese Academy of Sciences
Chinese Academy of Sciences
Beijing 100049, China

Supporting information for this article is available on the WWW under https://doi.org/10.1002/cnma.201800052

This manuscript is part of a Special Issue on Selective Nanocatalysis. Click here to see the Table of Contents of the special issue.

potential, diffuse on the support and attach to the larger ones with lower chemical potential. In earlier time, Wynblatt and Gjostein[16] generalized the Ostwald ripening theory of the particles in solution developed by Lifshitz, Slyozov,[17] and Wagner[18] (so called LSW theory) to the gas-solid interface. They defined the critical radius, a key parameter describing the ripening behaviour, under the interface-control and diffusion-control limit. Later on, a revised theory applicable to the small particle sizes was proposed.[19] More accurate evaluation of the critical radius subject to the mass conservation[20] and efficient algorithm allowing a larger time step to solve the rate equation[21] were developed. In presence of reactants, the ripening could be promoted significantly via the metal-reactant complexes, and corresponding theory was derived in our previous work.[22] In this context, formation of the metal-reactant complexes was subject to the metal-support interaction, and influence of reactant adsorption on surface energy of supported particles was included in corresponding ripening theory as well. These provide a unique framework to explore the influence of the metal-support interaction and surface energy on ripening kinetics.

We report here a theoretical investigation of influence of the metal-support interaction, surface energy and sublimation energy on Ostwald ripening of supported metal particles. Ostwald ripening under both isothermal and temperature programmed conditions were considered. Corresponding half-life time and onset temperature of ripening are extracted to quantify the dependence of the ripening resistance on the metal-support interaction, sublimation energy and surface energy.For metal-support interaction, we differentiate in particularly two different metal-support interactions, metal particle-support interaction (MPSI) and metal atom-support interaction (MASI). Surprisingly, these two MSIs present a completely different and actually opposite influence on rate of ripening, which is important for rational design of supported nano-catalysts.

Results and Discussion

Ripening under (Non)Isothermal Conditions

We first studied the ripening of supported metal particles with initial average curvature diameter $<d_0>=<2R_0>=3$ nm and relative standard deviation $rsd_0=16.7\%$ under the isothermal condition of 500 K. $E_{tot}=2.0$ eV, $\gamma=0.094$ eV/Å^2 and $\alpha=90^\circ$ were used in simulation. As expected, both the maximum and average diameter (Figure 1a) increases gradually with ripening time. The ratio between maximum and average diameter converges to about 1.25, consistent with the result of Ostwald ripening with LSW distribution of 1.333.[23] There is a little change in the standard deviation of PSD, in agreement with literature as well.[24] Evolution of the total volume, the particle number, and dispersion[25] (the ratio between surface atoms exposed and the total atoms of the supported particles) are plotted in Figure 1b. It can be found that the total volume remains constant, indicating that the total mass is conserved in simulation. We note that at the earlier stage of ripening, there is a large number of smaller particles with higher chemical potential, and the driving force for ripening is larger. As a result, the dispersion decreases more rapidly at beginning but becomes slowly later. Different from the dispersion, the particle number decay faster. Specifically, at the time for 50% decrease of dispersion, corresponding particle number drops down to almost 10% of its initial value. The reason behind is that the disappearance of smaller particles with less number of atoms contributes little to the variation of dispersion. Since variation of the particle number is more sensitive to time, corresponding half-life time $t_{1/2}$ is defined to quantify the sintering rate and facilitate the comparison below. In this particular case, corresponding half-life time is 50 days.

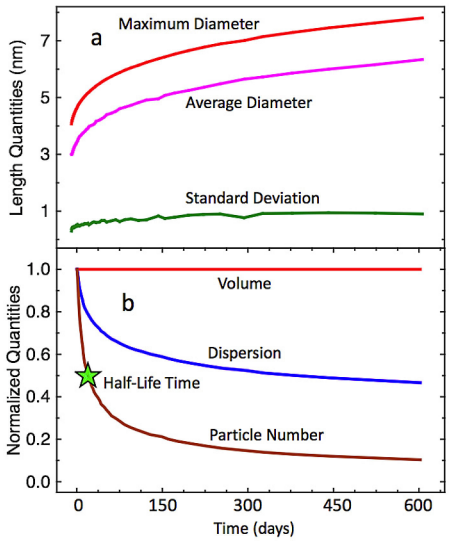

Figure 1. (a) Average and maximum diameter, standard deviation versus ripening time. (b) Normalized volume, dispersion and particle number versus ripening time, and half-life time (green star) is indicated. Thermal temperature = 500 K, $E_{tot}=2$ eV, $\alpha=90^\circ$, $v_s=6\times10^{13}$ s^{-1}, initial $<d_0>=<2R_0>=3$ nm, $rsd_0=16.7\%$, $\gamma=0.094$ eV/Å^2, $\Omega=18.27$ Å^3, the ratio between diffusion length and particle radius $L_r=1.2$.

Ostwald ripening under temperature programmed condition tells the thermal resistance, and the corresponding results are plotted in Figure 2. It can be found that the maximum and average diameter remains same with its initial value before 600 K, and afterward it starts to increase rapidly with ramping temperature (Figure 2a). Corresponding standard deviation shows a modest increase. In line with rapid increase of the average size, the dispersion and particle number decrease almost linearly with ramping temperature (Figure 2b). There is no pronounced decrease in ripening rate with further increase of ramping time, in contrast to those under the isothermal condition. This is because the influence from gradual increase in ramping temperature on ripening rate overwhelms that from the size increase. To characterize the thermal resistance, we defined onset temperature T_{on}, corresponding temperature for 10% decrease of the particle number with respect to its initial value. In this particular case, corresponding T_{on} is 635 K.

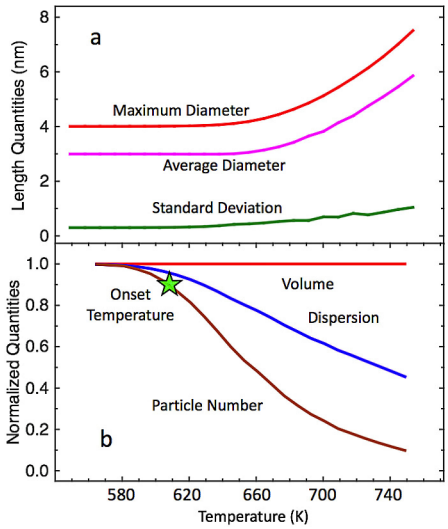

Figure 2. (a) Average and maximum diameter, standard deviation versus ramping temperature. (b) Normalized volume, dispersion and particle number versus ramping temperature, and onset temperature (green star) is indicated. Temerature ramping rate is 1 K/s and from 200 K. $E_{tot}=2$ eV, $\alpha=90^{\circ}$, $v_s=6\times10^{13}$ s^{-1}, initial $<d_0>=<2R_0>=3$ nm, $rsd_0=16.7\%$, $\gamma=0.094$ eV/Å^2, $\Omega=18.27$ Å^3, the ratio between diffusion length and particle radius $L_r=1.2$.

Metal Particle-Support Interaction (MPSI)

As indicates above, there are two types of metal-support interactions (MSI), namely, metal particle-support interaction (MPSI) and metal atom-support interaction (MASI). Both of them affect the ripening kinetics. On homogeneous support, MPSI and MASI are closely related, and the stronger MSI implies strong MPSI and MASI at same time. Whereas for inhomogeneous support, metal particle and atom could be distributed in different domains, MPSI and MMSI are not necessarily related. For general purpose, we treat them here as independent variables. This not only simplifies the analysis and also allows to quantify their relative importance on ripening kinetics. We applied this below for investigation of sublimation energy and surface energy as well.

We describe first the influence of MPSI. MPSI can be measured from the interface adhesion energy E_{adh} between metal particle and support, and is approximately here by their contact angle, based on Young–Dupré equation, $E_{adh}=\gamma(1+\cos\alpha)$. Though accurate determination of the contact angle remains elusive,[26] it varies from 45° to 135° for typical metal-oxide combinations as summarized in Table S1.[19c]

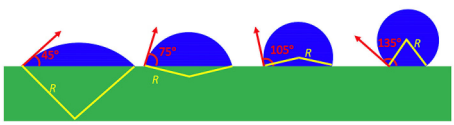

Figure 3. Four supported nanoparticles with different contact angle α from 45°, 75°, 105° to 135° with the same nanoparticle volume $V_p=16.76$ nm^3, corresponding curvature diameter $d\ (=2R)=8.2$, 4.7, 3.6, 3.2 nm, respectively.

For stronger MPSI, that contact angle is smaller, and the metal particles tend to spread on supports and maximize their contact area. For a particle with given volume, this means that corresponding curvature radius would increase with gradual increase of MPSI. In Figure 3, four spherical particles with same volume but different contact angles of 135°, 105°, 75° and 45° are plotted, and corresponding curvature diameter ($d=2R$) increases from 3.2, 3.59, 4.69 to 8.2 nm.

MPSI influences further on the prefactor A(R) and chemical potential term $\Delta\mu(R)$ in rate equation and therefore the overall ripening rate. As indicated above, the prefactor (Eq. 2) is related to the ripening mechanism (interface or diffusion control) and geometrical factor proportional to the perimeter length between particle and support. From Figure 4a, it can be found

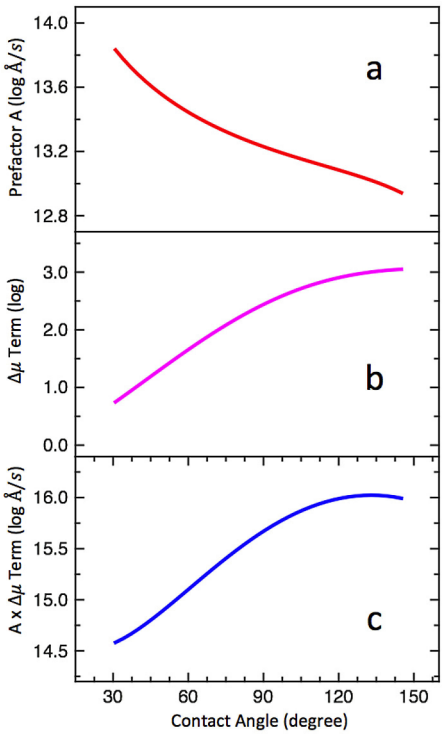

Figure 4. The prefactor $A(R)$ (a), exponential term of chemical potential $\Delta\mu$ (b) and their product (c) versus the contact angle α for a supported particle under the same particle volume $V_p=16.76$ nm^3, the ratio between diffusion length and particle radius $L_r=1.2$, $\Omega=15.33$ Å^3, $E_{tot}=3$ eV, $v_s=6\times10^{13}$ s^{-1}, initial $rsd_0=10\%$, $\gamma=0.094$ eV/Å^2, isothermal temperature $T=800$ K.

that prefactor $A(R)$decreases with the contact angle. Since weak MPSI (large contact angle) would result in small curvature radius, the corresponding chemical potential $\Delta\mu(R)$ increases. This would raise the driving force of ripening, a fact that increases the ripening rate. Variation of the chemical potential term in rate equation versus the contact angle is plotted in Figure 4b, and indeed it increases monotonically with the contact angle (weakening MPSI). Compared to the prefactor part, the change of chemical potential part is pronounced. Their overall contribution to the ripening rate is therefore determined mainly by the chemical potential part (Figure 4c). As a result, stronger MPSI (small contact angle) decreases the ripening rate,

and increases the ripening resistance, well proving physical intuition.

Figure 5a shows the particle number evolution with ripening time for these four contact angles considered. It can be found that with decreasing α from 135° to 45° or strengthening MPSI, the decay curve is right shifted and postponed. Namely, the stronger MPSI indeed improves the ripening resistance. Half-life time $t_{1/2}$ at wide range of contact angle were calculated and plotted in Figure 5b. For the contact angle decreasing from 135°~105°, its influence on $t_{1/2}$ is modest. This is understandable since corresponding MPSI is weak. While with further decrease of α, $t_{1/2}$ increases gradually, as expected. In overall, influence of MPSI on calculated half-life time falls in range of three orders of magnitude.

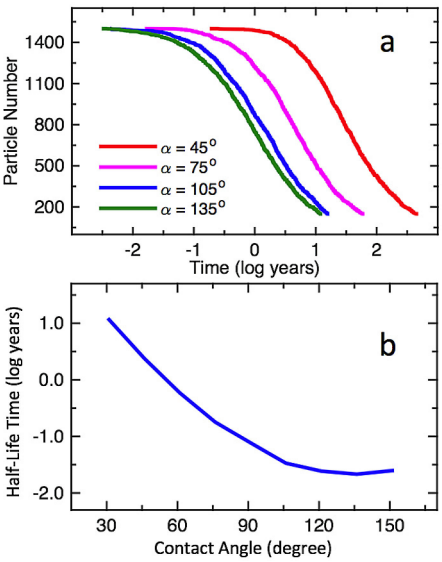

Figure 5. (a) Particle number evolution with time at $\alpha = 45°$, 75°, 105°, 135° and corresponding initial curvature diameter $<d> = 7.7$ nm, 4.4 nm, 3.4 nm, 3.1 nm. (b) Calculated half-life time $t_{1/2}$ versus the contact angle. Initial average particle volume $<V_P> = 14.14$ nm^3, relative standard deviation $rsd_0 = 10\%$, $\gamma = 0.159$ eV/Å^2, $E_{tot} = 3$ eV, $v_s = 6\times10^{13}$ s^{-1}, isothermal temperature $T = 800$ K.

barrier. According to density functional theory calculation on transition metal atoms adsorption on oxide surfaces,[27] the absolute value of E_b can be as large as a few electron volts or so. Whereas on stoichiometric surfaces, the corresponding diffusion barriers E_d vary modestly and falls typically around or even less than one electron volt.[28] This is understandable since there is much less number of bond making and breaking involved in diffusion, compared to the binding of the metal atom toward the oxide surfaces. Compared to E_d, E_b is decisive and sensitive to MASI. We therefore focus below influence of E_b on ripening for given E_{sub} and E_d. We note that surface defects such as vacancies and/or step edge can significantly hinder the diffusion and even stabilize the single atoms,[29] and its influence to the overall ripening is however beyond scope of the present work.

Figure 6 shows calculated onset temperature T_{on} and half-life time $t_{1/2}$ at different binding energies. It can be found that both the onset temperature and logarithm of half-life time decrease linearly with increase of the binding strength. Specifically, T_{on} and $t_{1/2}$ decrease by about 1000 Kelvin and more than 10 orders of magnitude. For comparison, the results at different contact angles are plotted. By decreasing the contact angle, calculated onset temperature and half-life time upshift constantly. Namely, stronger MPSI does improve the ripening resistance, as already revealed above. However, the extent of upshift falls in range of two hundred Kelvin and three orders of magnitude, much less than those of MASI.

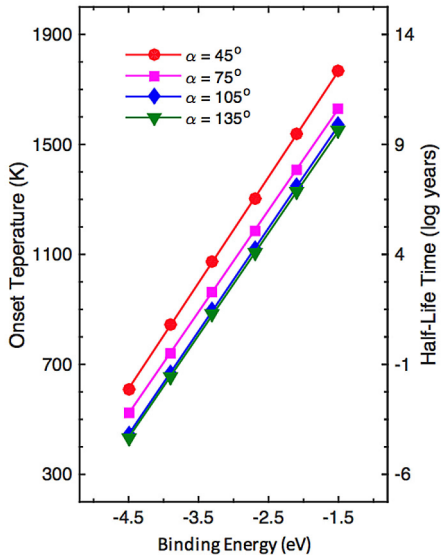

Figure 6. Calculated onset temperature T_{on} and half-life $t_{1/2}$ of supported particles versus the binding energy E_b at different contact angle. Initial average particle volume $<V_P> = 14.14$ nm^3 and $rsd_0 = 10\%$, $\gamma = 0.159$ eV/Å^2, $E_{sub} = 5.64$ eV, $E_d = 0.5$ eV, $v_s = 6\times10^{13}$ s^{-1}. Temperature ramping rate is 1 K/s and from 200 K, isothermal temperature $T = 800$ K.

Metal Atom-Support Interaction (MASI)

Metal atom-support interaction (MASI) determines the total activation energy $E_{tot} = E_d + E_f$, the summation of the diffusion barrier E_d and the formation energy E_f (with respect to infinite bulk counterpart) of the metal atoms on supports.[22] The formation energy can be derived from the sublimation energy (E_{sub}, endothermic) of bulk metal and the binding energy of the metal atom in gas phase on the substrate (E_b, exothermic), namely, $E_f = E_{sub} + E_b$.[19] For given metal (and so for E_{sub}), E_{tot} becomes a function of E_b and E_d, which are determined explicitly by MASI.

For given metal, depending on oxide surfaces, MASI might vary considerably, and so for the binding energy and diffusion

Above results show firmly that compared to MPSI, MASI is the key to the ripening. Strong MASI increases dramatically the ripening rate, a fact that should be prevented for the overall stability of supported particles. This is understandable since

MPSI mainly influences the prefactor and the difference of exponential function of the chemical potential in rate equation, whereas MASI determines the total activation energy and influences exponentially the corresponding ripening rate. Interestingly, interplay between MPSI and MASI was found recently to play an important role on the stability of single atom catalysts.[29]

Sublimation Energy and Surface Energy

Above results show the importance of metal-support interaction on the ripening kinetics. We investigate here the influence of metal composition and surface energy on the ripening kinetics. The influence of the composition is represented here by the sublimation energy E_{sub}. Actually, sublimation energy varies in a considerable range of value from 2.83 eV (Mn) to 8.48 eV (W), as seen from Table S2. We therefore investigated its impact on onset temperature and half-life time by fixing other parameters in rate equation.

As shown in Figure 7, with increasing E_{sub} from 4 eV to 7 eV, T_{on} and $t_{1/2}$ significantly increase by about 1000 K and more

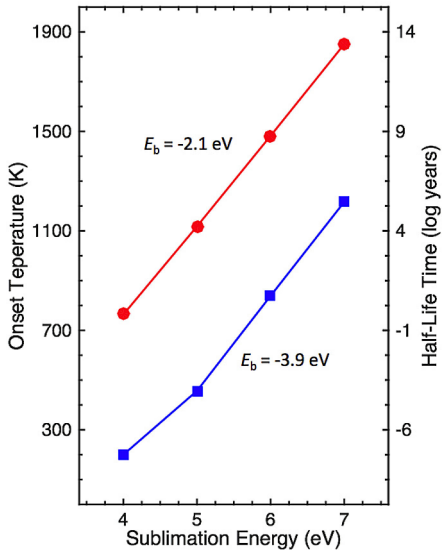

Figure 7. Calculated onset temperature T_{on} and half-life $t_{1/2}$ of supported particles versus the total activation energy E_{tot} at given binding energy E_b. Initial average curvature diameter $<d>=3.8$ nm and $rsd_0=10\%$, $\alpha=90^\circ$, $\gamma=0.159$ eV/Å^2, $E_d=0.5$ eV, $v_s=6\times10^{13}$ s^{-1}. Temperature ramping rate is 1 K/s and from 200 K, isothermal temperature $T=800$ K.

than 10 orders of magnitude. The sublimation energy of the supported metal particles has great impact on the ripening kinetics, as the binding energy of metal atom on support. Namely, the metal with higher sublimation energy would have a higher ripening resistance as well. At high temperature, ripening through gas phase might play a role. In this particular case, the catalysts with high sublimation energy become essential, and alloying the catalysts with metal having higher sublimation energy could be used to improve the ripening resistance.

Surface energy of supported particles influences the ripening kinetics because it affects the chemical potential of metal atoms in supported particles (Eq. 3). For large metal particle with specific morphology, the corresponding value can be obtained through experimental measurements.[19c] Alternatively, it can be estimated via weighted summation of surface energy of exposed facets.[22] Surface energy could depend further on composition[30] and size.[19a] In present work, it is input as a parameter, and we use the values from literature to estimate the range of surface energy. As shown in Table S2, it can be as lower as 0.056 eV/Å^2 for La and as higher as 0.228 eV/Å^2 for Re.[30] The influence of surface energy on the ripening kinetics is plotted in Figure 8. It can be found that with increase

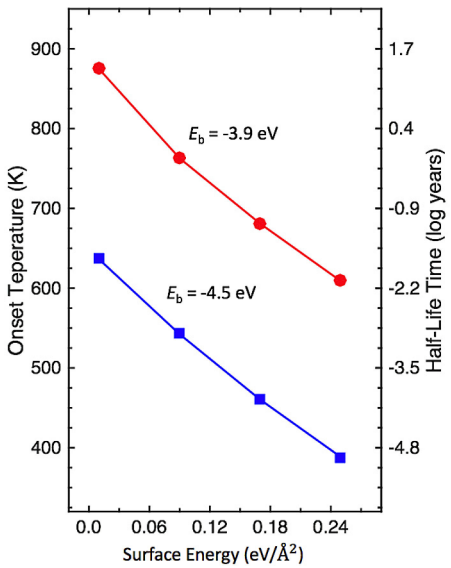

Figure 8. Calculated onset temperature T_{on} and half-life $t_{1/2}$ of supported particles versus the surface energy at different binding energy E_b. Initial average curvature diameter $<d>=3.8$ nm and $rsd_0=10\%$, $\alpha=90^\circ$, $E_{sub}=5.64$ eV, $E_d=0.5$ eV, $v_s=6\times10^{13}$ s^{-1}. Temperature ramping rate is 1 K/s and from 200 K, isothermal temperature $T=800$ K.

of the surface energy from 0.01 to 0.25 eV/Å^2, onset temperature decreases by about 300 Kelvin and half-life time decreases by about 3 orders of magnitude. Namely, higher surface energy would have relative lower ripening resistance. This is understandable since the higher the surface energy, the higher the chemical potential of supported particles.

Under reaction conditions, the surface energy could be lowered due to adsorption of reactants. For Rh(111), calculated clean surface energy was 0.172 eV/Å^2, and after adsorption of CO, it reduced considerably by 0.08 eV/Å^2.[22] According to above result, this would stabilize the corresponding particles and improve the ripening resistance. On the other hand, depending on the metal-reactant interaction and metal-support interaction, the reactants might not only stabilize the supported particles but also the metal atom on support via formation of the metal-reactant complexes. To form favourable metal-reactant complexes, corresponding total activation energy for

ripening is lowered, a fact that would promote significantly the ripening as well.[5d,31]

Based on above result, we consider explicitly the half-life time and onset temperature with respect to the total activation energy from 1.6 to 4.8 eV, and the results at different contact angles of 45°, 75°, 105°, 135° are plotted in Figure 9. It is clear

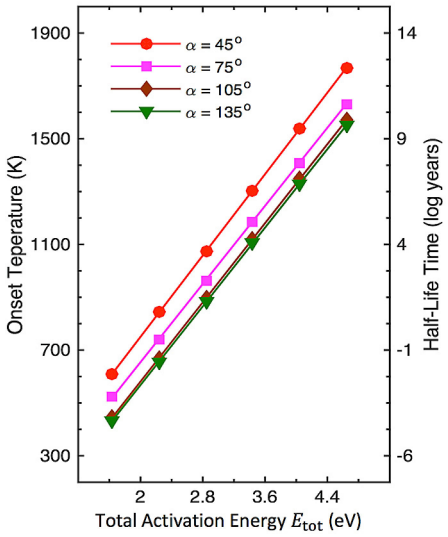

Figure 9. Calculated onset temperature T_{on} and half-life $t_{1/2}$ of supported particles versus the total activation energy E_{tot} at different contact angle α. Initial average particle volume $<V_p>=14.14$ nm^3 and $rsd_0=10\%$, $\gamma=0.159$ eV/Å^2, $E_{sub}=5.64$ eV, $E_d=0.5$ eV, $v_s=6\times10^{13}$ s^{-1}. Temperature ramping rate is 1 K/s and from 200 K, isothermal temperature $T=800$ K.

that the ripening kinetics is highly sensitive to the total activation energy decided by MASI, but much less sensitive to the contact angle decided by MPSI. We note that weak MSI would decrease MASI and increase the total activation energy, which is therefore effective to decrease the ripening rate. On the other hand, weak MSI would decrease MPSI and facilitate the particle migration and coalescence at the same time, a fact that is undesired. How to balance these two distinct metal-support interaction are crucial to the overall stability of supported particles and is under investigation.

Conclusions

We studied theoretically the influence of metal-support interaction, sublimation energy and surface energy on ripening risistance of supported particles. The ripening kinetics was simulated under both isothermal and temperature programmed conditions, and trend variation of corresponding half-life time and onset temperature of ripening at wide range of the phase space were quantified. It is found that though the metal particle-support interaction (small contact angle) and lower surface energy could stabilize the supported particles, their influence on the ripening resistance is relative modest. In contrast, the strong metal atom-support interaction decreases the total activation energy of ripening, worsering dramatically the ripening resistance. Moreover, it is found that the submlimation energy also have a great influence on the ripening resistance. For Ostwald ripening alone, we conclude that the metal atom-support interaction, instead the metal particle-support interaction, is decisive, a fact that should be prevented. The interplay between these two-distinct metal-support interactions plays an important role in the overall stability of supported catalysts and calls for further study in future.

Method for Kinetic Simulation

Theory of Ostwald ripening for supported particles can be found in earlier work,[16b,19b,22] and we brief here the key points for convenience. For particle at a given curvature radius R, corresponding rate equation under steady state is

$$\left(\exp\left[-\frac{E_{tot}}{kT}\right]\right)\left(\exp\left[\frac{\Delta\mu_{NP}(R^*)}{kT}\right]-\exp\left[\frac{\Delta\mu_{NP}(R)}{kT}\right]\right) \quad (1)$$

Above equation consists of three parts, namely, the prefactor part $A(R)$, total activation energy part (E_{tot}) and exponential term of chemical potential $\Delta\mu$. Prefactor $A(R)$ is related with the ripening mechanism and sensitively depends on the shape and size of supported particles.

$$A(R)=\frac{XY}{X+YR^2}\frac{K}{} \quad (2)$$

where $X=2\pi a_0 R\sin(\alpha)$, $Y=2\pi a_0{}^2/\ln[L/R\ \sin(\alpha)]$ and $K=\nu_s\Omega/[4\pi a_0{}^2\alpha_1]$. α is contact angle between metal NP and support, which reflects metal particle-support interaction (MPSI). a_0 is the lattice constant of the support surface, L is the diffusion length of the monomer, ν_s is the vibrational frequency of the monomer on the support surface, Ω is the molar volume of bulk metal atom, $\alpha_1=(2-3\cos\alpha+\cos^3\alpha)/4$ is geometrical factor, k is Boltzmann constant, T is temperature. When $X\gg Y$, the ripening is diffusion control, and when $X\ll Y$, it is interface control.

Total activation energy E_{tot} is the summation of formation energy E_f of the metal atom (with respect to the bulk counterpart) and corresponding diffusion barrier E_d on support. This term is decided by the metal atom-support interaction (MASI), which will be addressed in this contribution. Chemical potential $\Delta\mu$ part describes the growth direction of the particles. Here, chemical potential $\Delta\mu$ is the energy of the atom in particle of interest with respect to the bulk counterpart. In the present work, it is approximated by Gibbs-Thomson (G–T) relation[16b,19b]

$$\Delta\mu(R)=\frac{2\ \Omega\gamma}{R} \quad (3)$$

γ is the surface energy of supported metal particles. It is sensitive to composition,[30b] dependent on the particle size,[19b]

and could be mediated further by the metal-support interaction[9a,26,32] and adsorption of reactants.[22] In present work, variation of the surface energy with the particle size in the process of growth is neglected for simplicity.

Initial particle size distribution (PSD) of supported particles is assumed here to follow a Gaussian distribution $f(R, t)$ with average size of $<R>$ and standard deviation σ. Mass conservation indicates

$$\frac{4}{3}\pi\alpha_1 \int_0^\infty f(R,t)R^3 dR = V_0 \quad (4)$$

where V_0 is the initial total volume of supported metal particles. The particle number $N(t)$ evolves with rime as below

$$N(t) = \int_0^\infty f(R,t)dR \quad (5)$$

For a particle at a given radius of $R=d/2$ (d is particle diameter), whether it grows or shrinks is decided by the particle at the critical radius R^* depicted in Eq. 1. The particle at the critical radius R^* implies there is no net change in mass, size and morphology etc for corresponding particle. When $R>R^*$, the rate is positive and the corresponding particle will grow. Obviously, R^* increases gradually with time, and should be decided efficiently during the ripening. So far, there is no analytic formula beyond the interface and diffusion control limits available yet. One has to determine R^* numerically.[20–21] We note that the amount of catalysts is assumed mass conserve, namely, there is no catalyst loss and gain. As a result, R^* should be solved under the constrain of mass conservation. Once the critical radius is derived, a proper time step in Eq. 1 should be given for increasing or decreasing certain value of the size for each individual particle. Too small time-step would be time consuming, whereas too large time-step might break the mass conservation. On the other hand, for Ostwald ripening at lower temperature or having a higher total activation energy, the corresponding rate is rather slow, and a larger time-step is desirable to save the computational time. Whereas for ripening at higher temperature or having a lower total activation energy, the ripening process could be very fast, and the time-step could be smaller. To meet all these requirements, we adopted an efficient self-adapted time-step algorithm under the constraint of the mass conservation. One unique feature of the algorithm is that the iteration of bisection method is nested into the iteration of self-adapt time step technology, which allows the critical radius and the time-step can be determined simultaneously.

Ripening kinetics under isothermal and temperature programmed aging (TPA) condition are considered, and corresponding dispersion, particle number and average size are calculated. For the isothermal condition, the thermal temperature used in the present work is 500 or 800 K, while for TPA, the initial temperature is 200 K, and the temperature ramping rate is 1 K/s.

Supporting Information

Supporting Information is available from the Wiley Online Library or from the author.

Acknowledgements

We acknowledge funding from the Chinese Academy of Sciences (QYZDJ-SSW-SLH054), the Natural Science Foundation of China (91645202), and the National Key R&D Program of China (2017YFB0602200).

Conflict of Interest

The authors declare no conflict of interest.

Keywords: Ostwald ripening · Metal support interaction · Kinetics · Nanoparticles

[1] A. T. Bell, *Science* **2003**, *299*, 1688–1691.
[2] a) C. H. Bartholomew, *Appl. Catal. A* **2001**, *212*, 17–60; b) J. A. Moulijn, A. E. van Diepen, F. Kapteijn, *Appl. Catal. A* **2001**, *212*, 3–16.
[3] a) M. Valden, X. Lai, D. W. Goodman, *Science* **1998**, *281*, 1647–1650; b) I. Lee, F. Delbecq, R. Morales, M. A. Albiter, F. Zaera, *Nat. Mater.* **2009**, *8*, 132–138; c) W. Zhu, R. Michalsky, O. Metin, H. Lv, S. Guo, C. J. Wright, X. Sun, A. A. Peterson, S. Sun, *J. Am. Chem. Soc.* **2013**, *135*, 16833–16836; d) X. F. Yang, A. Q. Wang, B. T. Qiao, J. Li, J. Y. Liu, T. Zhang, *Acc. Chem. Res.* **2013**, *46*, 1740–1748.
[4] a) D. Kandel, *Phys. Rev. Lett.* **1997**, *79*, 4238–4241; b) M. José-Yacamán, C. Gutierrez-Wing, M. Miki, D. Q. Yang, K. N. Piyakis, E. Sacher, *J. Phys. Chem. B* **2005**, *109*, 9703–9711; c) G. Palasantzas, T. Vystavel, S. A. Koch, J. T. M. De Hosson, *J. Appl. Phys.* **2006**, *99*.
[5] a) C. G. Granqvist, R. A. Buhrman, *J. Catal.* **1976**, *42*, 477–479; b) A. K. Datye, Q. Xu, K. C. Kharas, J. M. McCarty, *Catal. Today* **2006**, *111*, 59–67; c) A. Howard, C. E. J. Mitchell, R. G. Egdell, *Surf. Sci.* **2002**, *515*, L504-L508; d) S. B. Simonsen, I. Chorkendorff, S. Dahl, M. Skoglundh, J. Sehested, S. Helveg, *J. Am. Chem. Soc.* **2010**, *132*, 7968–7975; e) G. S. Parkinson, Z. Novotny, G. Argentero, M. Schmid, J. Pavelec, R. Kosak, P. Blaha, U. Diebold, *Nat. Mater.* **2013**, *12*, 724–728; f) A. Berko, F. Solymosi, *J. Catal.* **1999**, *183*, 91–101; g) A. Kolmakov, D. W. Goodman, *Rev. Sci. Instrum.* **2003**, *74*, 2444; h) A. Berkó, J. Szökő, F. Solymosi, *Surf. Sci.* **2004**, *566–568, Part 1*, 337–342; i) D. E. Starr, S. K. Shaikhutdinov, H. J. Freund, *Top. Catal.* **2005**, *36*, 33–41; j) M. Di Vece, D. Grandjean, M. J. Van Bael, C. P. Romero, X. Wang, S. Decoster, A. Vantomme, P. Lievens, *Phys. Rev. Lett.* **2008**, *100*; k) F. Yang, M. S. Chen, D. W. Goodman, *J. Phys. Chem. C* **2009**, *113*, 254–260; l) S. R. Challa, A. T. Delariva, T. W. Hansen, S. Helveg, J. Sehested, P. L. Hansen, F. Garzon, A. K. Datye, *J. Am. Chem. Soc.* **2011**, *133*, 20672–20675; m) S. B. Simonsen, I. Chorkendorff, S. Dahl, M. Skoglundh, K. Meinander, T. N. Jensen, J. V. Lauritsen, S. Helveg, *J. Phys. Chem. C* **2012**, *116*, 5646–5653; n) J. Sehested, A. Carlsson, T. V. W. Janssens, P. L. Hansen, A. K. Datye, *J. Catal.* **2001**, *197*, 200–209; o) J. Sehested, *J. Catal.* **2003**, *217*, 417–426; p) R. S. Goeke, A. K. Datye, *Top. Catal.* **2007**, *46*, 3–9; q) S. B. Simonsen, I. Chorkendorff, S. Dahl, M. Skoglundh, J. Sehested, S. Helveg, *J. Catal.* **2011**, *281*, 147–155.
[6] a) C. T. Campbell, J. R. V. Sellers, *Chem. Rev.* **2013**, *113*, 4106–4135; b) F. Qiang, L. Wei-Xue, Y. Yunxi, L. Hongyang, S. Hai-Yan, M. Ding, G. Xiang-Kui, C. Limin, W. Zhen, Z. Hui, W. Bing, B. Xinhe, *Science* **2010**, *328*, 1141–1144.
[7] T. W. Hansen, A. T. Delariva, S. R. Challa, A. K. Datye, *Acc. Chem. Res.* **2013**, *46*, 1720–1730.
[8] Y. Nagai, T. Hirabayashi, K. Dohmae, N. Takagi, T. Minami, H. Shinjoh, S. i. Matsumoto, *J. Catal.* **2006**, *242*, 103–109.
[9] a) J. A. Farmer, C. T. Campbell, *Science* **2010**, *329*, 933–936; b) N. Ta, J. J. Liu, S. Chenna, P. A. Crozier, Y. Li, A. Chen, W. Shen, *J. Am. Chem. Soc.*

2012, *134*, 20585–20588; c) C. T. Campbell, *Acc. Chem. Res.* **2013**, *46*, 1712–1719; d) S. J. Tauster, *Acc. Chem. Res.* **1987**, *20*, 389–394.
[10] a) Q. Fu, W.-X. Li, Y. Yao, H. Liu, H.-Y. Su, D. Ma, X.-K. Gu, L. Chen, Z. Wang, H. Zhang, B. Wang, X. Bao, *Science* **2010**, *328*, 1141–1144; b) Q. Fu, F. Yang, X. Bao, *Acc. Chem. Res.* **2013**, *46*, 1692–1701.
[11] a) D. W. Goodman, *Catal. Lett.* **2005**, *99*, 1–4; b) A. Bruix, J. A. Rodriguez, P. J. Ramírez, S. D. Senanayake, J. Evans, J. B. Park, D. Stacchiola, P. Liu, J. Hrbek, F. Illas, *J. Am. Chem. Soc.* **2012**, *134*, 8968–8974; c) C. T. Campbell, *Nat. Chem.* **2012**, *4*, 597–598; d) X. Liu, M.-H. Liu, Y.-C. Luo, C.-Y. Mou, S. D. Lin, H. Cheng, J.-M. Chen, J.-F. Lee, T.-S. Lin, *J. Am. Chem. Soc.* **2012**, *134*, 10251–10258.
[12] a) S. J. Tauster, S. C. Fung, R. L. Garten, *J. Am. Chem. Soc.* **1978**, *100*, 170–175; b) G. L. Haller, D. E. Resasco, in *Adv. Catal., Vol. Volume 36* (Eds.: H. P. D. D. Eley, B. W. Paul), Academic Press, **1989**, pp. 173–235.
[13] a) W. Yan, B. Chen, S. M. Mahurin, E. W. Hagaman, S. Dai, S. H. Overbury, *J. Phys. Chem. B* **2004**, *108*, 2793–2796; b) M. T. Bore, H. N. Pham, E. E. Switzer, T. L. Ward, A. Fukuoka, A. K. Datye, *J. Phys. Chem. B* **2005**, *109*, 2873–2880.
[14] C. L. Kuo, K. C. Hwang, *Chem. Mater.* **2013**, *25*, 365–371.
[15] a) T. Uchiyama, H. Yoshida, Y. Kuwauchi, S. Ichikawa, S. Shimada, M. Haruta, S. Takeda, *Angew. Chem. Int. Ed.* **2011**, *50*, 10157–10160; b) F. Mittendorfer, N. Seriani, O. Dubay, G. Kresse, *Phys. Rev. B* **2007**, *76*; c) K. P. McKenna, A. L. Shluger, *J. Phys. Chem. C* **2007**, *111*, 18848–18852.
[16] a) P. Wynblatt, *Acta Metall.* **1976**, *24*, 1175–1182; b) P. Wynblatt, N. A. Gjostein, *Acta Metall.* **1976**, *24*, 1165–1174.
[17] I. M. Lifshitz, V. V. Slyozov, *J. Phys. Chem. Solids* **1961**, *19*, 35–50.
[18] C. Wagner, *Zeitschrift für Elektrochemie, Berichte der Bunsengesellschaft für physikalische Chemie* **1961**, *65*, 581–591.
[19] a) C. T. Campbell, S. C. Parker, D. E. Starr, *Science* **2002**, *298*, 811–814; b) S. C. Parker, C. T. Campbell, *Phys. Rev. B* **2007**, *75*, 035430; c) C. T. Campbell, J. R. V. Sellers, *Faraday Discuss.* **2013**, *162*, 9–30.
[20] L. R. Houk, S. R. Challa, B. Grayson, P. Fanson, A. K. Datye, *Langmuir* **2009**, *25*, 11225–11227.
[21] F. Behafarid, B. Roldan Cuenya, *Surf. Sci.* **2012**, *606*, 908–918.
[22] R. Ouyang, J. X. Liu, W. X. Li, *J. Am. Chem. Soc.* **2013**, *135*, 1760–1771.
[23] P. Wynblatt, N. A. Gjostein, *Prog. Solid State Chem.* **1975**, *9*, 21–58.
[24] J. J. Li, C. W. Guo, Y. Ma, Z. J. Wang, J. C. Wang, *Acta Mater.* **2015**, *90*, 10–26.
[25] Q. Xu, K. C. Kharas, B. J. Croley, A. K. Datye, *ChemCatChem* **2011**, *3*, 1004–1014.
[26] S. L. Hemmingson, C. T. Campbell, *ACS Nano* **2017**, *11*, 1196–1203.
[27] a) B. R. Goldsmith, E. D. Sanderson, R. Ouyang, W.-X. Li, *J. Phys. Chem. C* **2014**, *118*, 9588–9597; b) X. D. Li, Y. M. Fang, S. Q. Wu, Z. Z. Zhu, *AIP Adv.* **2015**, *5*; c) S. Fernandez, A. Markovits, F. Fuster, C. Minot, *J. Phys. Chem. C* **2007**, *111*, 6781–6788; d) G. Yu, M. Zhu, Y. Zheng, *J. Mater. Chem. C* **2014**, *2*, 9767–9774; e) W. S. A. Halim, A. S. Shalabi, K. A. Soliman, *Int. J. Quantum Chem.* **2009**, *109*, 1094–1102.
[28] a) H. Iddir, S. Ogut, N. D. Browning, M. M. Disko, *Phys. Rev. B* **2005**, *72*, 4; b) L. Xu, G. Henkelman, C. T. Campbell, H. Jónsson, *Surf. Sci.* **2006**, *600*, 1351–1362; c) G. Barcaro, A. Fortunelli, *New J. Phys.* **2007**, *9*, 22; d) R. Meyer, Q. F. Ge, J. Lockemeyer, R. Yeates, M. Lemanski, D. Reinalda, M. Neurock, *Surf. Sci.* **2007**, *601*, 134–145.
[29] J. C. Liu, Y. G. Wang, J. Li, *J. Am. Chem. Soc.* **2017**, *139*, 6190–6199.
[30] a) L. Vitos, A. V. Ruban, H. L. Skriver, J. Kollár, *Surf. Sci.* **1998**, *411*, 186–202; b) K. F. Wojciechowski, *Surf. Sci.* **1999**, *437*, 285–288.
[31] J. L. Lu, H. J. Gao, S. Shaikhutdinov, H. J. Freund, *Catal. Lett.* **2007**, *114*, 8–16.
[32] S. C. Parker, C. T. Campbell, *Top. Catal.* **2007**, *44*, 3–13.

Manuscript received: February 4, 2018
Version of record online: ■■, ■■■